Received: 16 May 2022 | Revised: 12 July 2022 | Accepted: 20 July 2022

DOI: 10.1111/ijac.14269

International Journal of Applied Ceramic Technology

SPECIAL ISSUE ARTICLE

Critical thickness of polymer-derived ceramic coatings with particulate fillers

Zhao Zhang | **Rajendra K. Bordia** | **Fei Peng**

Department of Materials Science and Engineering, Clemson University, Clemson, South Carolina, USA

Correspondence
Rajendra K. Bordia and Fei Peng, Department of Materials Science and Engineering, Clemson University, Clemson, SC 29634, USA.
Email: rbordia@clemson.edu and fpeng@clemson.edu

Funding information
US Department of Energy; National Energy Technology Lab, Grant/Award Number: DE-FE003128; GE Gas Power; National Science Foundation, Grant/Award Number: OIA-1655740

Abstract

In this study, we demonstrate a novel environmental barrier coating processed from polymer-derived ceramics (PDCs) with homogeneously distributed submicrometer Y_2O_3 as the filler. Under suitable conditions, dense and crack-free coatings can be achieved for all the designed compositions with the volumetric content of Y_2O_3 varied from 45 to 93 vol%. To process the PDC SiC–Y_2O_3 composite coatings, Y_2O_3 particles and SiC liquid precursor were uniformly dispersed in hexane and then dip-coated on SiC substrates. After cross-linking at 250°C and heat-treated at 900°C in argon, dense and crack-free PDC SiC–Y_2O_3 composite coatings were formed. The effect of coating thickness and heat-treatment temperature on the formation of cracks due to constrained pyrolysis was studied. The critical thickness for realizing crack-free coatings of three compositions (i.e., 93, 77, and 45 vol% Y_2O_3) was studied for heat treatment from 1000 to 1300°C using atomic force microscope and scanning electron microscopy. As heat-treatment temperature increases, the critical coating thickness decreases for the same coating compositions due to enhanced shrinkage at higher temperature. With higher Y_2O_3 content, the critical thickness of the coating increased. The inert Y_2O_3 particles reduce the amount of polymer leading to reduction in the overall constrained shrinkage of the coating during heat treatment.

KEYWORDS
ceramics, coating, critical thickness, polymer-derived ceramics, yttrium oxide

1 | INTRODUCTION

Films and coatings are used widely to modify the physical and chemical properties of a surface or substrate. The high mechanical properties (e.g., modulus, hardness, wear, and strength) and chemical stabilities of ceramic materials make ceramic coatings attractive candidates for protections against wear, oxidation, and corrosion.[1–3] To realize the desired performance of ceramic coatings, it is important to control the coating thickness.[4–7] Coatings that are too thin will not be able to provide enough protection against wear and corrosion. On the other hand, if the coatings are too thick, cracks will form and propagate resulting in coating failure.

During the processing of coatings, there is a "critical thickness."[8–11] The coating will be dense and crack-free below the critical thickness and has cracks above it. This can be explained by an energy balance between the surface energy required to create a new crack surface and the strain energy released as a crack grows.[12] For ceramic

coating, especially for the application of corrosion protection, a dense and crack-free coating is a requirement. Therefore, it is important to study the critical thickness of different coating compositions and heat-treatment conditions. In this paper, we investigate how powder dispersibility, filler content, drying process, and heat-treatment temperature affect the critical coating thickness of polymer-derived ceramic (PDC) SiC–Y_2O_3 composite coatings.

PDCs are silicon-based amorphous ceramic materials obtained from organic precursors. PDCs have been used to make SiC-based ceramic coatings, fibers, bulk, and cellular ceramics.[13–15] The PDC route is especially attractive to make coatings at relatively low temperatures. However, the primary challenge of this approach is the significant shrinkage during the polymer-to-ceramic conversion. One way to compensate for the high shrinkage is to introduce active or passive fillers in the preceramic precursor.[16–21] Passive fillers, such as BN,[22,23] YSZ,[24] Al_2O_3,[25,26] ZrO_2,[18,27] will stay inert through the polymer-to-ceramic conversion. They reduce coating shrinkage simply by reducing the volume fraction of the shrinking polymer phase.[21] Active fillers, such as Al,[26,28] Si,[26] TiB_2,[29] $ZrSi_2$,[27] react with the precursor, decomposition products of the polymer, or atmosphere.[21] For appropriately chosen fillers, the volume expansion of the reaction can additionally compensate for the polymer shrinkage.[30]

In addition, fillers can also be used to design and tailor the thermal,[31] mechanical,[32] and electrical[33,34] properties of PDCs. For example, in a recent study, Y_2O_3 powder was added to polysiloxanes to make yttrium silicate coatings for the protection of C/SiC composites from recession in dry air or water vapor. It showed excellent oxidation protection.[35] Most recently, Y_2O_3 and Yb_2O_3 powders were added to polysilazanes to make yttrium and ytterbium silicates coatings for hot gas oxidation protection of Si_3N_4.[36]

In this study, PDC SiC–Y_2O_3 composite coatings were processed by adding Y_2O_3 filler to polycarbosilane, a precursor for SiC. The Y_2O_3 content was varied in the composite coatings (between 45 and 93 vol%). This allows the future development of polymer-derived functional graded coating,[37–40] which smoothly transitions from a bottom bond interface that contains almost pure SiC, to a top surface that contains a high content of Y_2O_3. This graded environmental barrier coating (EBC) system is being developed in our lab to protect SiC_f/SiC substrates against high-velocity steam attack. A dense top layer of Y_2O_3 has low oxygen permeability and high corrosion resistance under high-velocity steam. Even if a certain degree of oxidation occurs within this innovative EBC, Y_2O_3 can react with silica forming yttrium silicate, which can still provide excellent stability and oxidation protection.[41]

TABLE 1 Sample name and corresponding volumetric compositions of the polymer-derived ceramic (PDC) SiC–Y_2O_3 composites

Sample name	Solvent	Total ceramic yield (grams per 1 g suspension)	Y_2O_3 (vol%)	PDC SiC (vol%)
Y100	Hexane	.6	100	0
Y93S	Hexane	.6	93	7
Y77S	Hexane	.6	77	23
Y45S	Hexane	.6	45	55
S100	Hexane	.6	0	100

Abbreviation: PDC, polymer-derived ceramic.

2 | EXPERIMENTAL PROCEDURES

In this study, the SiC precursor was SMP-10 (StarPCS, Schenectady, NY). The Y_2O_3 filler was yttrium(III) oxide nanopowder (50–70 nm, 99.995%, Alfa Aesar, MA). Five compositions were investigated, as shown in Table 1. To measure the density of PDC SiC, SMP-10 was cross-linked and pyrolysized at 900°C. The density of pyrolysized ceramic was measured using a helium pycnometer (AccuPyc 1330, Micromeritics, Norcross, GA). The measured density of PDC-derived amorphous SiC was 2.94 g/cm^3. This, together with the theoretical density of Y_2O_3 (5.01 g/cm^3), was used for the calculation of theoretical density of the composites and for the conversion of weight percentages to volume percent for the composite coating composition.

The flowchart of the coating processing is shown in Figure 1. To prepare the uniformly dispersed Y_2O_3/SMP-10 suspensions, first, hexane was mixed with an SiC precursor. Overall, 5 wt% dispersant (Efka FA 4608, BASF, Charlotte, NC) based on the weight of Y_2O_3 nanoparticles was also added and mixed thoroughly by a magnetic stirrer. Then yttrium(III) oxide nanopowder (50–70 nm, 99.995%, Alfa Aesar, MA) was added into the solvent and ball-milled for 72 h. Finally, the slurry was homogenized using a high-energy ultrasonication probe for 2 h with 100% power (1s on + 1s pause) (Vibra-Cell VC500, Sonics, CT). The amount of hexane, Y_2O_3, SMP-10 needed in this step was calculated based on Table 1, assuming that the ceramic yield of 1 g SMP-10 is .767 g after heat treatment (discussed in Section 3). During heat treatment, all of the hexane and the dispersant evaporated completely.

The viscosity of Y_2O_3-SMP-10 suspensions was determined by a viscometer (Brookfield DV3THBCJ0, Ametek Brookfield, Middleboro, MA) at a shear rate between 115.2 and 960 s^{-1} at room temperature. The density was calculated by the measured weight of the fixed volume of suspension in a liquid pycnometer (25 ml) using an analytical balance (PI-214, Denver Instrument Co., Denver,

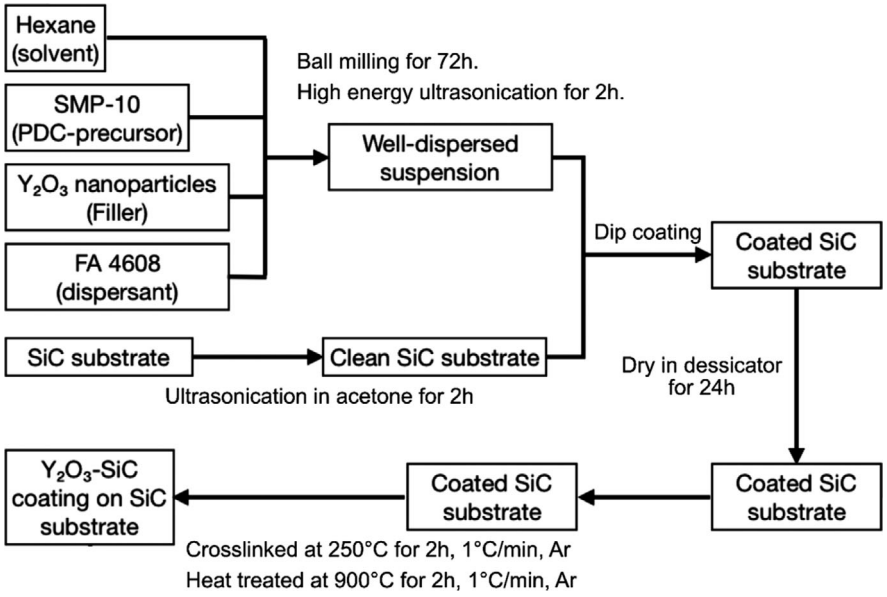

FIGURE 1 Flowchart for the experimental approach of fabrication of Y_2O_3 − −SiC coating on SiC substrate

CO). Silicon carbide (4H N type S, MSE Supplies, AZ) was used as the substrate for dip-coating. SiC substrates were first ultrasonicated in acetone for 2 h then rinsed with acetone and DI water. The substrates were subsequently dried thoroughly before dip-coating.

Various compositions of Y_2O_3/SiC coatings were prepared (Table 1) on the cleaned surface of an SiC substrate by the dip-coating method and their microstructures after heat treatment were investigated. Dip-coating was carried out using the following steps: The substrates were first immersed in the suspension at a constant speed of 100 mm/min, held in the suspension for 10 s, and then withdrawn at various speeds ranging from 10 to 500 mm/min to get different coating thicknesses.[42,43] The dip-coating was conducted in a KVS NIMA dip coater (Biolin Scientific, Espoo, Finland). The coating was dried for 24 h in a desiccator at room temperature before heat treatment. Room temperature and a desiccator were used for low-rate controlled drying, which was needed to avoid drying cracks.

The coatings were cross-linked at 1°C/min to 250°C for 2 h followed by heat treatment at a heating rate of 1°C/min to 900°C for 2 h to complete the polymer-to-ceramic conversion. To test the temperature dependence of critical thickness, the pyrolyzed coating was heated to target temperatures (1000, 1100, 1200, and 1300°C) at 5°C/min. Once the target temperature was achieved the power was cut off, and coated substrate was furnace cooled to room temperature. All heat-treatment processes, including cross-linking, were performed under ultrahigh purity flowing argon in a tube furnace (CM Furnaces, Bloomfield, USA).

X-ray diffraction (XRD) was used to analyze the sintered sample. XRD measurements were performed on a Rigaku MiniFlex 600 powder diffractometer (XRD, Rigaku MiniFlex 600 X-ray generator, Cu K_α radiation, $\lambda = 1.5406$ Å). Data were digitally recorded in a continuous scan in the range of angle (2θ) from 20° to 80° with a scanning rate of 1°/min. The microstructures of the heat-treated coatings were then observed by scanning electron microscopy (SEM, Hitachi S4800, Hitachi, Ltd., Tokyo, Japan) and an optical microscope (BX60, Olympus). The thickness of the heat-treated coatings was measured using an atomic force microscope (AFM, Alpha300, WITec Instruments Corp.). Scratches were made on the films using a metal blade after heat treatment. AFM measurements were carried out to obtain the height difference between the coating and the substrate.

The pyrolysis and mass change behavior of the pure cross-linked SMP-10 powders were investigated by thermogravimetric analysis (Netzsch STA 449 F3 Jupiter) up to 1400°C at a rate of 1°C/min under argon atmosphere. The weight change of pure SMP-10 before and after cross-linking was also measured using an analytical balance (PI-214, Denver Instrument Co., Denver, CO).

3 | RESULTS AND DISCUSSION

The viscosities of the slurries, as a function of the shear rate, are shown in Figure 2. The pure Y_2O_3 slurry demonstrated shear thinning behavior. After mixing with SMP-10, the viscosity became significantly lower and Newtonian. It is interesting that the viscosities of all slurries of SMP-10

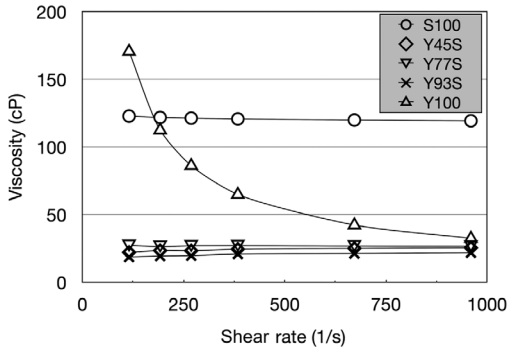

FIGURE 2 The viscosities of the slurries as a function of shear rate

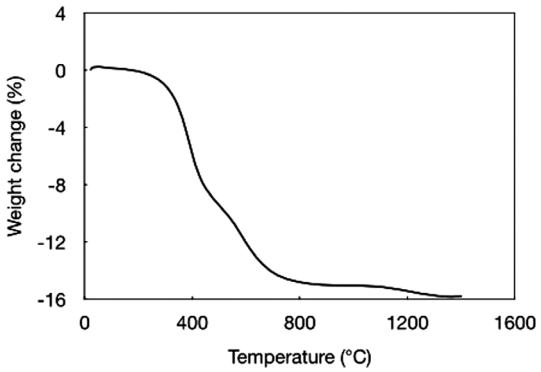

FIGURE 3 Thermogravimetric analysis of the cross-linked SMP-10 powders up to 1400°C with a heating rate of 2.5°C/min under flowing argon

and Y_2O_3 are lower than that of pure SMP-10, and that of pure Y_2O_3. This suggests interaction between SMP-10 and Y_2O_3 particles. Further analysis is needed to explain this observation.

The thermal behavior of the cross-linked SMP-10 powders was characterized by TGA in argon at a temperature up to 1400°C with a heating rate of 1°C/min. The TGA result (Figure 3) shows that the total weight loss, during pyrolysis of the cross-linked polymer, was approximately 15.77%. The weight loss began near 350°C, indicating the pyrolysis process of SMP-10. Majority of the weight loss occurs below 800°C with a small amount of weight loss in the 1100–1250°C range. The mass change during cross-linking at 250°C in argon was 9% resulting in a total mass loss of 23.3% (from the liquid polymer to pyrolyzed ceramic). Therefore, the ceramic yield of SMP-10 after pyrolysis was 76.7%.

3.1 | Crystalline phases

Figure 4 shows the XRD pattern of the Y_2O_3/SMP-10 composite powders after heat treatment at various

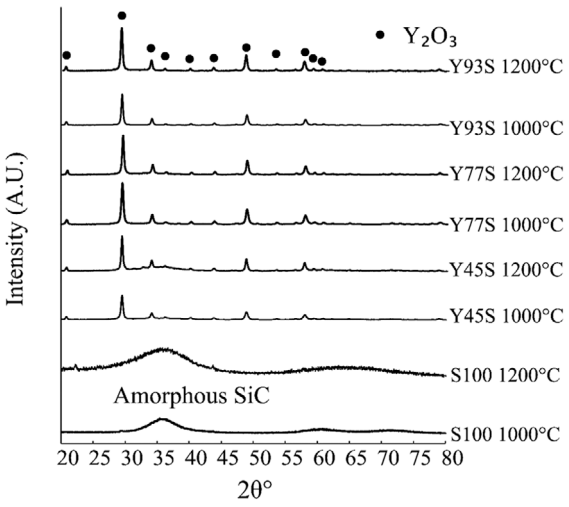

FIGURE 4 X-ray diffraction (XRD) patterns of composite powders heat-treated in argon flow

temperatures. It revealed that the only crystalline phase in the powder after the heat treatment is Y_2O_3. Neither yttrium monosilicate nor yttrium disilicate formed during the heat treatment. The broad hump between 30° and 40° verified the existence of amorphous SiC phase.

3.2 | The effect of slurry formulation and preparation on slurry stability and coating morphology

The effect of the particle dispersing method on the slurry stability and coating morphology was investigated to determine optimal dispersing method. There different approaches to disperse the particles in the precursor were investigated: (A) a high-energy planetary ball milling (Vertical Planetary Ball Mill, MA0101, MSE Supplies, AZ) for 4 h; (B) regular ball milling for 72 h and then ultrasonication (VWR Ultrasonic Cleaner 97043-964, 35 kHz, 90 W, Radnor, PA) for 2 h; (C) regular ball milling for 72 h and then high-energy ultrasonication for 2 h with 100% power (1s on + 1s pause) (Vibra-Cell VC500, Sonics, CT). Figure 5 depicts the results of different mixing methods on slurry stability after 4 h of sedimentation. Surprisingly, high-energy planetary ball milling resulted in the worst suspension, with nanoparticles agglomerated and sedimented. High-energy milling leads to increased surface area and this may result in agglomeration. In contrast, high-energy probe ultrasonication resulted in the most stable dispersed slurry. This was selected as the final step to obtain well-dispersed Y_2O_3 nanoparticle suspensions after ball milling. We also investigated the effect of the amount of dispersant on slurry quality. Overall, 3–10 wt% dispersant, Efka FA 4608 (BASF, Charlotte, NC) based on

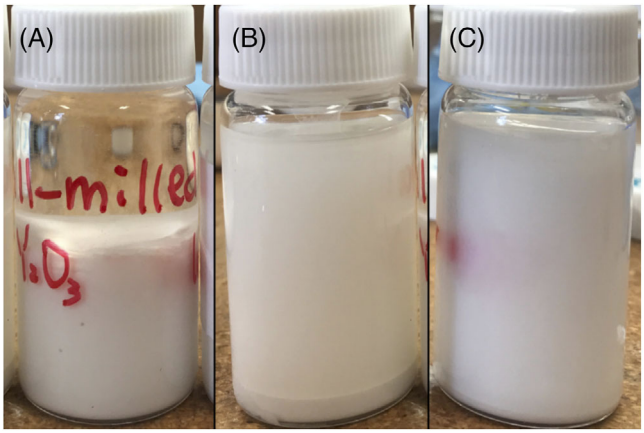

FIGURE 5 Y_2O_3 (40 wt%) suspensions in hexane with 3% Efka 4608 prepared by different mixing methods after 4-h sedimentation: (A) high-energy planetary ball milling; (B) ball milling + ultrasonication; (C) ball milling + high-energy ultrasonication for 2 h

the weight of Y_2O_3 nanoparticles was added and mixed thoroughly by a magnetic stirrer. We found the best combination for solvent and dispersant was 5% Efka 4608 in hexane (Figure 6).

The state of dispersion of the Y_2O_3 particles in the suspension has a significant effect of the coatings' quality. When the Y_2O_3 nanoparticles were not well dispersed or not distributed homogenously in the suspension, extensive cracking occurred during pyrolysis (Figure 7). This is because cracks could form and propagate within the polymer-derived ceramics, where the local shrinkage is much higher than regions where Y_2O_3 nanoparticles are distributed. Another possible reason for the poor quality may be nonuniform coating thickness.

3.3 | Microstructure

Further studies were conducted using the optimized slurry formulation—dispersant was 5 wt% (based on the weight of Y_2O_3)—Efka 4608 in hexane and particle dispersion method (regular ball milling for 72 h and then high-energy ultrasonication for 2 h with 100% power [1s on + 1s pause]). These studies were conducted to investigate the effect of composition on the microstructure. Figure 8 shows the results obtained after heat treatment at 900°C. For sample Y100, there is clear evidence of lack of sintering as the coating has significant porosity. In contrast to sample Y100, the other three compositions with PDC-SiC formed dense films. Yttria nanopowders were dispersed in the amorphous dense SiC matrix. As expected, at this low heat-treatment temperature, no significant grain growth of yttria nanopowder was observed for all compositions. Interestingly, with a higher content of yttria nanopowder, the uniformity of the film improved. The uniformity of the yttria nanopowder distribution indicates that the slurries remained well dispersed during the coating process.

To investigate the composition of the amorphous phase connecting yttria nanopowders, EDX was conducted (Figure 9). The result shows the main elements were silicon, carbon, and yttrium. Oxygen was also present in the selected field. It is possible there was some oxidation in the amorphous phase. However, combined with the XRD results (Figure 4), we believe it is more likely that the oxygen signal was contributed from the Y_2O_3 particles embedded in the amorphous phase.

3.4 | The effect of the filler content and heat-treatment temperature on critical thickness

In most cases, cracking in the coatings could be observed visually or using optical microscope. This is because, due to the large pyrolysis shrinkage, the cracks due to constrained pyrolysis have much larger crack opening displacement compared to thermal expansion mismatch cracks (origin is low differential thermos-elastic strains). The crack opening displacement is a clear way to differential between cracking due to constrained sintering or pyrolysis and cracking due to thermal expansion mismatch between the coating and substrate.[8]

In some cases, with micro-cracks, SEM investigation was needed. For any coating, which did not show cracks visually or in optical microscope, we conducted SEM to ensure they were indeed crack-free. Figure 10 shows an example of the crack-free coating and cracked coating under SEM.

In Figure 11, the effect of volume fraction of Y_2O_3 and the heat-treatment temperature on the critical coating thickness is plotted. Coatings from the three compositions (Y93S, Y77S, and Y45S) were prepared with different thicknesses and heat-treated at different temperatures. After heat treatment, the coatings were examined to determine if they had cracks or not (either optically or optically and SEM). Based on these, observation data are plotted in Figure 11 with a "cross" for coatings that showed cracks, and a "circle" for the ones that did not show cracking. Figure 11 is thus a process map identifying conditions under which robust crack-free coatings can be produced. The amount of Y_2O_3 had the dominant effect on the critical coating thickness. At all heat-treatment temperatures from 1000 to 1300°C, Y93S had the highest critical thickness. For example, for heat treatment at 1000°C, the critical

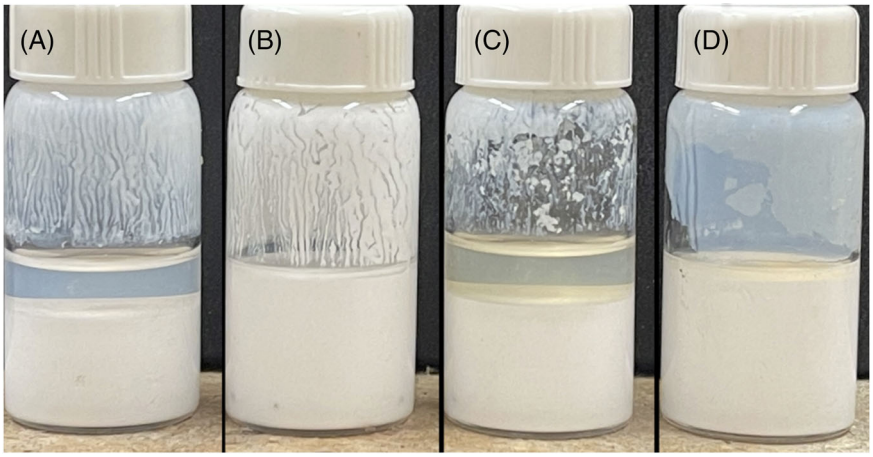

FIGURE 6 The dispersibility of Y_2O_3 (60 wt%) suspensions in hexane, with different concentrations of dispersant, after 2 h of sedimentation: (A) 3% Efka 4608; (B) 5% Efka 4608; (C) 8% Efka 4608; (D) 10% Efka 4608

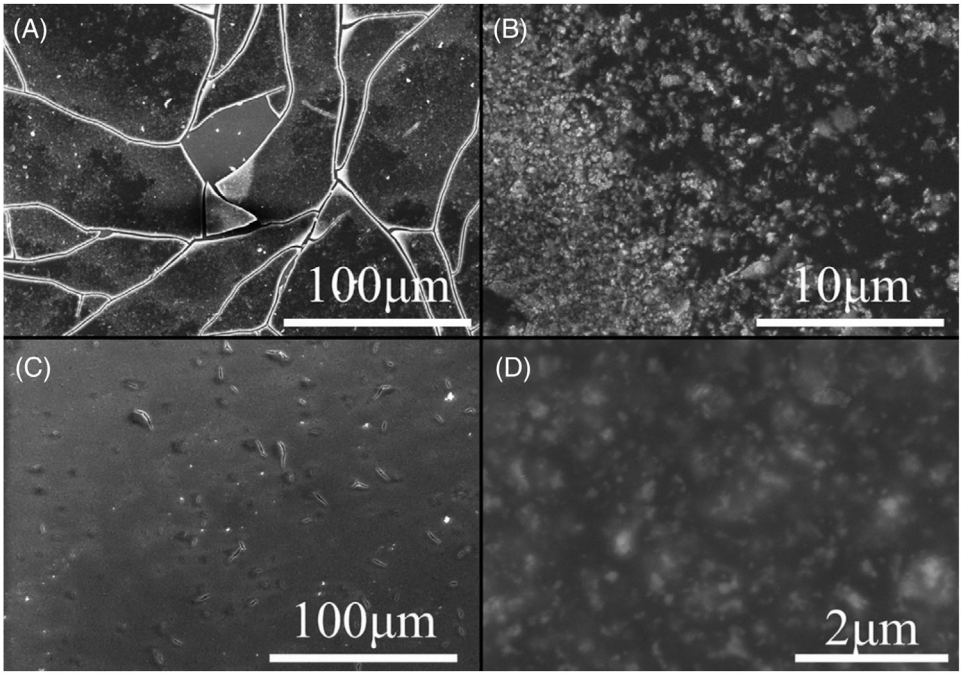

FIGURE 7 Microstructure of pyrolyzed ceramic coatings: (A) and (B) ceramic coatings using poorly dispersed slurries; (C) and (D) ceramic coatings using well dispersed slurries. In both cases, the composition is Y45S, and the coatings were heat treatment at 1000°C.

thicknesses are ~1220 nm for Y45S, ~1330 nm for Y77S, and ~2280 nm for Y93S.

The effect of Y_2O_3 content is expected because the fraction of shrinking polymer component decreases as the amount of Y_2O_3 increases. The total volume change during pyrolysis can be calculated using the following equation[15]:

$$\Psi_{\text{total}} = \left(1 - \frac{V_f}{V_f^{\max}}\right)\left(\Psi_p - 1\right) + V_f\left(\Psi_f - 1\right) + V_P \quad (1)$$

where V_f, V_P are the filler volume fraction and pore volume fraction, respectively, Ψ_P, Ψ_f are the specific volume change of the polymer and filler, respectively; and $V_f^{\max}$ is the max volume fraction of filler corresponding to the highest packing density of the filler.

For all three compositions, the critical thickness for a dense, crack-free coating decreased with temperature. From Figure 10, as the crack opening displacements are large, it is clear that these cracks occur due to pyrolysis shrinkage and not thermal expansion mismatch.[21] For SMP-10, Figure 3 shows the mass loss as a function of temperature. The majority of the mass loss is at temperature less than 1000°C. However, there was slight mass loss in a 1100–1200°C region. Although shrinkage was not measured, the shrinkage of the polymer is expected to be high at temperature less than 1000°C. For the composite coatings, we also need to consider the shrinkage

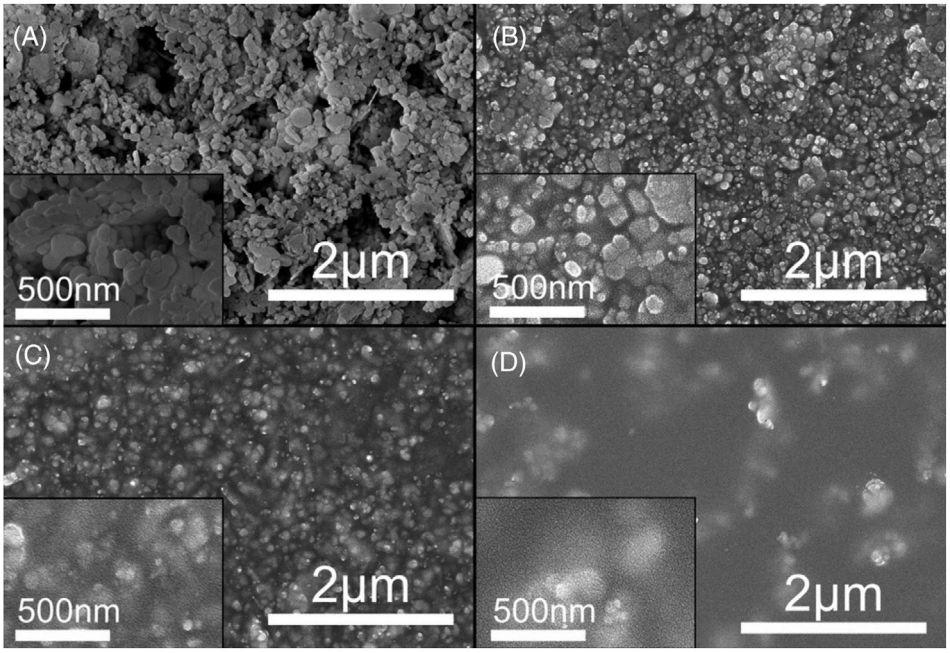

FIGURE 8 The morphology of dip-coated SiC substrate after heat treatment at 900°C in argon: (A) Y100, (B) Y93S, (C) Y77S, and (D) Y45S

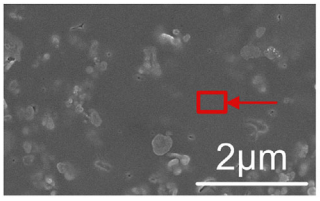

Element	Atomic %
C	31.55
O	15.42
Si	53.03

FIGURE 9 Scanning electron microscopy (SEM) and EDX image for sample Y45S heat-treated in argon at 1100°C. The red rectangle in the image shows the selected EDX inspection field.

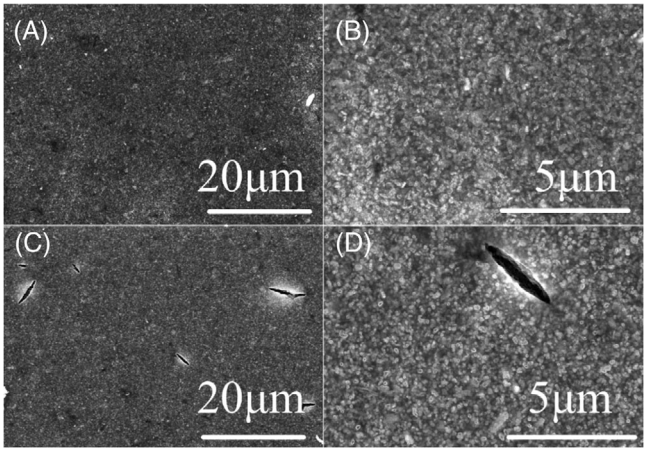

FIGURE 10 Scanning electron microscopy (SEM) images of crack free coating: parts (A) and (B) versus cracked coating parts (C) and (D). (A) and (B) Y77S, heat-treated at 1100°C, in argon, thickness = 935 nm; (C) and (D) Y77S, heat-treated at 1100°C, in argon, thickness = 985 nm

of Y_2O_3 due to sintering. This is expected to be dominant above 1200°C. The effect of temperature on the critical thickness (Figure 11) is explained by considering the combination of the shrinkage of polymer and sintering of Y_2O_3. For the films with high Y_2O_3 content (Y93S), there are two distinct regimes of decrease in critical thickness as a function of temperature. The first corresponds to the shrinkage of polymer (temperature < 1000°C), and the second corresponds to the densification of Y_2O_3 (temperature > 1200°C). For the high content of SMP-10 (Y45S), there was only one primary regime (temperature < 1000°C). The critical thickness of Y77S showed two regimes, but not as clearly as that for Y93S.

3.5 | The effect of solvent evaporation during drying process

In coating fabricated from particle suspension, cracks can also be induced by stress built up during the drying process.[44] For hard particles, such as ceramic powders, the tendency of cracking can be reduced by decreasing the solvent's surface tension, evaporation rate, or increasing the mechanical properties of the particles.[10] However, it is not particularly important to choose a solvent with a low evaporation rate in our system. Even in the event when the solvent evaporates quickly, the PDC precursor will remain fluid before cross-linking. The fluidity of the precursor helps to relieve the shrinkage stress during an

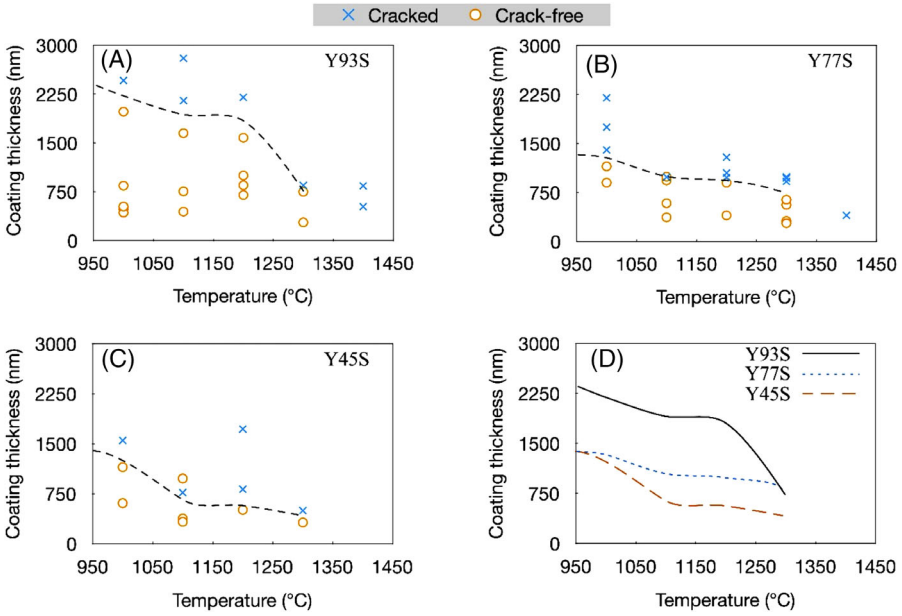

FIGURE 11 Process map for coatings. Coating integrity (cracked or not cracked) as a function of heat-treatment temperature for coatings of different compositions: (A) Y93S, (B) Y77S, (C) Y45S, (D) comparison of three compositions

evaporation of the solvent.[45] Additionally, the polymer precursor works as a binder of the Y_2O_3 particles, which helps to avoid cracking during drying.

4 | CONCLUSIONS

This study was focused on an investigation of the effect of the three important parameters on the processing of polymer-derived composite coatings—the composition of the composite, the coating thickness, and the heat-treatment temperature. Slurries of the polymer precursor for SiC and Y_2O_3 nanoparticles were dispersed by optimizing the solvent, amount of dispersant, and dispersion method. Using dip-coating and controlling the withdrawal speed, coatings of different thicknesses were made. After cross-linking and heat treatment, a composite coating with PDC-derived amorphous SiC matrix and Y_2O_3 nanoparticles as second phase was obtained. The only crystalline phase, detected by XRD, was Y_2O_3 up to a temperature of 1200°C.

After heat treatment, under certain conditions, cracks were observed in the coatings. From the wide crack opening displacement, it was concluded that the cracking occurs during polymer pyrolysis and sintering of Y_2O_3. It is due to the stresses induced during pyrolysis and sintering due to the in-plane constraint on the shrinkage from the substrate. The coating thickness has a dominant effect on whether a coating cracks or not. As the thickness increases, the tendency for crack formation increases. Critical coating thicknesses, such that the coatings do not crack if the thickness is below this value, were obtained for the composite coatings as a function of temperature and composition. For all compositions, the critical coating thickness decreases as heat-treatment temperature increases. This is because as heat-treatment temperature increases, the shrinkage of the composite system increases. There are two temperature regimes in which the behavior is different due to the origin of the shrinkage of the composite. At lower temperature, less than 1000°C, the shrinkage occurs primarily due to the pyrolysis of the polymer. At temperature greater than 1200°C, the shrinkage is controlled by the densification of the Y_2O_3 nanoparticles. Beyond 1200°C, the polymer pyrolysis is complete, and additional shrinkage in the polymer is negligible. The coating composition also has an important effect. At a fixed pyrolysis temperature up to 1300°C, the critical coating thickness increases as the amount of Y_2O_3 nanoparticles. This is because as the amount of Y_2O_3 increases, the amount of the polymer decreases, and this results in lower overall shrinkage as up to 1300°C, the dominant shrinkage is from the pyrolysis of the polymer.

ACKNOWLEDGMENTS

The authors would like to acknowledge support for this research from US Department of Energy, National Energy Technology Lab (award no. DE-FE003128), and GE Gas Power. This work was also supported in part by the National Science Foundation EPSCoR Program under NSF award no. OIA-1655740. Any opinions, findings, and conclusions or recommendations expressed in this material are those of the author(s) and do not necessarily reflect

those of the Department of Energy or the National Science Foundation. We also acknowledge discussion with Dr. Sanat Chandra Maiti and Dr. Quan Li.

ORCID

Rajendra K. Bordia https://orcid.org/0000-0001-9256-0301

REFERENCES

1. Cao XQ, Vassen R, Stoever D. Ceramic materials for thermal barrier coatings. J Eur Ceram Soc. 2004;24:1–10.
2. Schulz U, Peters M, Bach FW, Tegeder G. Graded coatings for thermal, wear and corrosion barriers. Mater Sci Eng A. 2003;362(1–2):61–80.
3. Wachtman JB. Mechanical and thermal properties of ceramics: proceedings. vol. 303. U.S. Government Printing Office, Washington, D.C., USA: US Department of Commerce, National Bureau of Standards; 1969.
4. Baraka R. Thickness dependence of electrical and optical properties of sol gel ZnO coatings. Asian J Chem. 2003;15:1729–34.
5. Li B, Fan X, Li D, Jiang P. Design of thermal barrier coatings thickness for gas turbine blade based on finite element analysis. Math Prob Eng. 2017;2017:1–13.
6. Dai H, Zhong XH, Li HY, Zhang YF, Meng J, Cao XQ. Thermal stability of double-ceramic-layer thermal barrier coatings with various coating thickness. Mater Sci Eng A: Struct Mater Prop Microstruct Process. 2006;433:1–7.
7. Liang LH, Liu XH, Chen LF, Wei YG. Effect of ceramic coating thickness on fracture behaviour of coating structure under thermal shock cycles. Ceram Int. 2022;48(8):11435–44.
8. Bordia RK, Jagota A. Crack growth and damage in constrained sintering films. J Am Ceram Soc. 1993;76:2475–85.
9. Lee WP, Routh AF. Why do drying films crack? Langmuir. 2004;20(23):9885–8.
10. Singh KB, Tirumkudulu MS. Cracking in drying colloidal films. Phys Rev Lett. 2007;98:218302.
11. Tirumkudulu MS, Russel WB. Cracking in drying latex films. Langmuir. 2005;21:4938–48.
12. Routh AF. Drying of thin colloidal films. Rep Prog Phys. 2013;76:046603.
13. Colombo P, Mera G, Riedel R, Sorarù GD. Polymer-derived ceramics: 40 years of research and innovation in advanced ceramics. J Am Ceram Soc. 2010;93:1805–37.
14. Greil P. Near net shape manufacturing of polymer derived ceramics. J Eur Ceram Soc. 1998;18:1905–14.
15. Greil P. Polymer derived engineering ceramics. Adv Eng Mater. 2000;2:339–48.
16. Dernovsek O, Bressiani JC, Bressiani AHA, Acchar W, Greil P. Reaction bonded niobium carbide ceramics from polymer-filler mixtures. 2000;35:2201–7.
17. Zhu YZ, Huang ZR, Dong SM, Yuan M, Jiang DL. Polymer-filler derived ceramics with low shrinkage using PCS/SiC/Al mixture. Physica status solidi (RRL) – rapid research letters. vol. 1. New Jersey: John Wiley & Sons Ltd; 2007. p. R59–61.
18. Günthner M, Schütz A, Glatzel U, Wang K, Bordia RK, Greißl O, et al. High performance environmental barrier coatings, Part I: Passive filler loaded SiCN system for steel. J Eur Ceram Soc. 2011;31(15):3003–10.
19. Wang KS, Gunthner M, Motz G, Bordia RK. High performance environmental barrier coatings, Part II: Active filler loaded SiOC system for superalloys. J Eur Ceram Soc. 2011;31(15):3011–20.
20. Fedorova A, Michelsen L, Scheffler M. Polymer-derived ceramic tapes with small and negative thermal expansion coefficients. J Eur Ceram Soc. 2018;38:719–25.
21. Barroso G, Li Q, Bordia RK, Motz G. Polymeric and ceramic silicon-based coatings – a review. J Mater Chem A. 2019;7:1936–63.
22. Morales JR. Manufacturing boron nitride nanotube (BNNT) reinforced polymer derived ceramic (PDC) composites for space applications. A thesis submitted to the Graduate Faculty of North Carolina State University in partial fulfillment of the requirements for the degree of Master of Science. Raleigh, North Carolina: North Carolina State University; 2021.
23. Günthner M, Kraus T, Krenkel W, Motz G, Dierdorf A, Decker D. Particle-filled PHPS silazane-based coatings on steel. Int J Appl Ceram Technol. 2009;6(3):373–80.
24. Petríková I, Parchovianský M, Švančárek P, Lenz Leite M, Motz G, Galusek D. Passive filler loaded polysilazane-derived glass/ceramic coating system applied to AISI 441 stainless steel, Part 1: Processing and characterization. Int J Appl Ceram Technol. 2019;17(3):998–1009.
25. Steinau M, Travitzky N, Gegner J, Hofmann J, Greil P. Polymer-derived ceramics for advanced bearing applications. Adv Eng Mater. 2008;10(12):1141–6.
26. Nguyen MD, Bang JW, Bin AS, Kim S-R, Kim Y, Hwang KH, et al. Novel polymer-derived ceramic environmental barrier coating system for carbon steel in oxidizing environments. J Eur Ceram Soc. 2017;37(5):2001–10.
27. Parchovianský M, Petríková I, Barroso G, Švančárek P, Galuskova D, Motz G, et al. Corrosion and oxidation behavior of polymer derived ceramic coatings with passive glass fillers on AISI 441 stainless steel. Ceramics-Silikáty. 2018;62(2):146–57.
28. Rocha RM, Bressiani JC, Bressiani AHA. Ceramic substrates of β-SiC/SiAlON composite from preceramic polymers and Al–Si fillers. Ceram Int. 2014;40(9):13929–36.
29. Jung S, Seo D, Lombardo SJ, Feng ZC, Chen JK, Zhang Y. Fabrication using filler controlled pyrolysis and characterization of polysilazane PDC RTD arrays on quartz wafers. Sens Actuators A. 2012;175:53–9.
30. Greil P. Active-filler-controlled pyrolysis of preceramic polymers. J Am Ceram Soc. 1995;78:835–48.
31. Barroso GS, Krenkel W, Motz G. Low thermal conductivity coating system for application up to 1000°C by simple PDC processing with active and passive fillers. J Eur Ceram Soc. 2015;35(12):3339–48.
32. Mirkhalaf M, Yazdani Sarvestani H, Yang Q, Jakubinek MB, Ashrafi B. A comparative study of nano-fillers to improve toughness and modulus of polymer-derived ceramics. Sci Rep. 2021;11(1):6951.
33. Ding D, Wang J, Yu X, Xiao G, Feng C, Xu W, et al. Dispersing of functionalized CNTs in Si–O–C ceramics and electromagnetic wave absorbing and mechanical properties of CNTs/Si–O–C nanocomposites. Ceram Int. 2020;46(4):5407–19.
34. Eichhorn F, Kellermann S, Betke U, Fey T. Phase evolution, filler-matrix interactions, and piezoelectric properties in lead zirconate titanate (PZT)-filled polymer-derived ceramics (PDCs). Materials (Basel). 2020;13(7):1520.

35. Liu J, Zhang LT, Hu F, Yang J, Cheng LF, Wang YG. Polymer-derived yttrium silicate coatings on 2D C/SiC composites. J Eur Ceram Soc. 2013;33(2):433–9.
36. Lenz Leite M, Barroso G, Parchoviansky M, Galusek D, Ionescu E, Krenkel W, et al. Synthesis and characterization of yttrium and ytterbium silicates from their oxides and an oligosilazane by the PDC route for coating applications to protect Si3N4 in hot gas environments. J Eur Ceram Soc. 2017;37:5177–91.
37. Liu J, Zhang L, Liu Q, Cheng L, Wang Y. Structure design and fabrication of environmental barrier coatings for crack resistance. J Eur Ceram Soc. 2014;34(8):2005–12.
38. Joshi SC, Ng HW. Optimizing functionally graded nickel–zirconia coating profiles for thermal stress relaxation. Simul Modell Pract Theory. 2011;19(1):586–98.
39. Zhang XC, Xu BS, Wang HD, Jiang Y, Wu YX. Application of functionally graded interlayer on reducing the residual stress discontinuities at interfaces within a plasma-sprayed thermal barrier coating. Surf Coat Technol. 2007;201(9–11):5716–9.
40. Basu SN, Kulkarni T, Wang HZ, Sarin VK. Functionally graded chemical vapor deposited mullite environmental barrier coatings for Si-based ceramics. J Eur Ceram Soc. 2008;28(2):437–45.
41. Liu J, Zhang L, Hu F, Yang J, Cheng L, Wang Y. Polymer-derived yttrium silicate coatings on 2D C/SiC composites. J Eur Ceram Soc. 2013;33:433–9.
42. Wang K, Bordia RK, Brush LN. A semi-empirical power-law model for the dip-coating of a substrate into a particle-containing, non-Newtonian, complex fluid system. Ceram Int. 2019;45(6):6655–64.
43. Zhang Z, Salamatin A, Peng F, Kornev KG. Dip coating of cylinders with Newtonian fluids. J Colloid Interface Sci. 2021;607(Part 1):502–13.
44. Xu P, Mujumdar AS, Yu B. Drying-induced cracks in thin film fabricated from colloidal dispersions. Drying Technol. 2009;27:636–52.
45. Lei H, Francis LF, Gerberich WW, Scriven LE. Stress development in drying coatings after solidification. AIChE J. 2002;48(3):437–51.

How to cite this article: Zhang Z, Bordia RK, Peng F. Critical thickness of polymer-derived ceramic coatings with particulate fillers. Int J Appl Ceram Technol. 2023;20:84–93. https://doi.org/10.1111/ijac.14269